RESEARCH ARTICLE







Check for updates

Basalt fiber reinforced polypropylene to manufacture 3D printed composites

Manuel Raul Pelaez-Samaniego^{1,2} | Kyleigh Rhodes^{2,3} | Tsai Garcia-Perez¹ Yu-Chung Chang² | Jinwen Zhang² | Muhammad Khusairy Bin Bakri² | Vikram Yadama² 🗅

¹Department of Applied Chemistry and Production Systems, Faculty of Chemical Sciences, University of Cuenca, Cuenca, Ecuador

²Composite Materials and Engineering Center, Washington State University, Pullman, Washington, USA

³Bio Materials, Willamette Valley Company, Eugene, Oregon, USA

Correspondence

Vikram Yadama, CMEC, Paccar 160, Washington State University, Pullman, USA.

Email: vyadama@wsu.edu

Funding information

National Science Foundation, Grant/Award Number: 1738669

Abstract

Polypropylene (PP) is one of the most used polymeric materials worldwide, either as a neat material or as a matrix for composite manufacture employing a molding process. Fused deposition modeling (FDM) 3D printing is an alternative process that offers the potential for manufacturing value-added products from PP. However, using neat PP for FDM is challenging because 3D-printed PP warps and shrinks when cooled, and the mechanical properties of PP are poor. PP-based composites with different fillers (e.g., glass, carbon, and natural fibers) have shown improved properties using FDM processes. An alternative filler for 3D-printed PP-based composites is basalt fiber (BF). The objective of this work was to assess the potential and impacts of BF as a filler for BF-PP composites using FDM processes. PP was compounded with 15, 25, 35, and 45 wt% BF to produce filaments for 3D printing without adding any compatibilizer. Results of rheology studies, morphology, and mechanical and thermal properties of the 3D printed specimens showed that BF positively impacts Young's modulus (E), thermal stability, and dimensional stability of the composite. All composites, when processed at high shear rates (i.e., above 100 1/s), show approximately similar rheological behavior. E is almost doubled in the composite with 25 wt% BF and increased fourfold in the composite with 35 and 45 wt% BF, compared to neat PP. The Izod impact resistance of the formulations containing 35 and 45 wt% BF is \sim 70% that of neat PP. BF process easily and adequately reinforces PP composites manufactured via FDM.

Highlights

- Neat PP's poor mechanical properties are improved by adding basalt fiber (BF).
- Up to 45 wt% BF was used to reinforce PP-based composites.
- PP-BF composites are easier to process via DFM compared to neat PP.
- BF improves PP-based composite's thermal and dimensional stability.

KEYWORDS

3D printing, basalt fiber, composites, fused deposition modeling, polypropylene

This is an open access article under the terms of the Creative Commons Attribution License, which permits use, distribution and reproduction in any medium, provided the original work is properly cited.

© 2024 The Author(s). Polymer Composites published by Wiley Periodicals LLC on behalf of Society of Plastics Engineers.





1 | INTRODUCTION

Polypropylene (PP) is one of the lightest and most flexible polymers, and thus, it is among the most used plastics globally. PP is widely employed in daily and technical products, including industrial fibers, textiles, packaging, food containers, medical devices, and dishware.² PP has also become one of the main thermoplastic materials in the automotive and aeronautics industries.^{3,4} PP is used either as a neat material or as a matrix for manufacturing composites, especially for non-structural applications. Recyclability is an important property of PP-based composites. 5,6 The main processes for industrially manufacturing PP-based composites are extrusion, injection molding, and compression molding.^{7–10} The filling materials for these composites include glass fiber (GF),¹¹ carbon fiber (CF),¹² Linz-Donawitz sludge, 13,14 lignocellulosic materials (e.g., flax, hemp, jute, or wood fibers),^{7,10} and cellulose.⁹ Wood plastic composites using PP have shown excellent resistance to natural weathering (i.e., exposure to ultraviolet light and humidity). 15

An alternative to injection molding, extrusion, or compression molding for manufacturing PP-based composites for specific applications is fused deposition modeling (FDM). FDM is a 3D printing process that has been identified as an important tool for producing customized parts for diverse applications, fast prototyping, mass customization, fabricating complex geometry parts in short periods, and minimizing waste. 16 Different parameters (e.g., infill density, build orientation, layer thickness, and type of infill) can affect the properties of the 3D-printed composite. 17 There is a growing interest in using FDM manufacturing to produce a variety of composites and different plastics and filler materials (e.g., CF, GF, and lignocellulosic fibers) have succeeded. The most used polymeric materials for FDM are polylactic acid (PLA) and acrylonitrile butadiene styrene (ABS), 5,18-20 but there is an increasing amount of works using nylon²¹ and polyethylene (PE).¹⁷ Thus, studies have explored the 3D printing of CF-reinforced ABS, ^{22–25} CF-reinforced PLA, ^{18,26} and CF and GF-reinforced nylon.^{17,27} However, only a few works have been conducted on 3D-printed PP-based composites. 2,5,28,29 High volumetric shrinkage and warpage are two recognized challenges for additive manufacturing of PP.30-33 Strategies for solving this problem include the use of fillers such as GF, CF, talc, 2,28,33 and natural fibers.⁵ In fact, commercially available PP filaments for 3D printing are not pure PP, but they include different formulations to improve PP 3D printability.³¹ Further strategies for making PP-based filaments more 3D printable can help to advance the use of PP for FDM. The addition of lignocellulosic fibers (LF) such as harakeke and hemp fibers, as well as synthetic fibers (e.g., GF and CF) in PP-based 3D-printed composites increases the mechanical properties of the composite, specifically Young's modulus.^{2,5,28} However, moisture adsorption, degradation, and limited temperature resistance can negatively affect the PP-LF composite's mechanical properties over time. Moreover, despite the positive effects of GF and CF as fillers for PP-based composites, CF is an expensive fiber and the use of GF introduces environmental limitations, especially for recycling.³⁴ Therefore, abundant, more environmentally friendly, and relatively cheaper alternatives to GF and CF are necessary.

One of the alternatives to CF and GF for filling PP-based composites is basalt fiber (BF). BF is a natural fiber of mineral origin, available worldwide, with high mechanical properties (tensile strength and elongation at break),³⁵ offering enormous potential as a substitute for GF and CF reinforcing fibers. BF possesses relatively better mechanical properties than traditional GF and is less costly than CF. 36,37 Also, the disposal and recycling of BF is less polluting than other fibers. ^{37,38} Furthermore, BF processing is expected to be less energy-intensive than other competing fibers, including GF.³⁵ Thus, BF is an excellent alternative to GF and CF in composite manufacture. The combination of important properties of PP (e.g., relatively low cost, low density, and resistance to chemicals)^{2,30,39} with those of BF (e.g., acid, alkali, moisture, biological, fire, UV light, and solvent resistance, low thermal conductivity, and nuclear radiation resistance)^{2,40} appears attractive for specific applications of the resulting composites. BF-PP composites can also be an option to solve the limitations of neat PP for 3D printing projects, such as the difficulty of acquiring adequate dimensional stability of 3D-printed PP² and PP's poor mechanical properties. Moreover, large amounts of PP are available worldwide, especially for recycling, because PP is one of the main components of plastic waste. 40 The use of BF with ABS for FDM has shown a positive impact of BF on the composite's mechanical properties.⁴¹ Nevertheless, the possibility of using FDM for PP-BF composites deserves more study. The work of Ghabezi et al.²⁹ is, to the best of our knowledge, one of the few that assessed the possibility of producing BF-PP 3D composites. The work used recycled PP and BF content up to 8 wt%, with a positive impact on the composite's mechanical properties. No compatibilizer was added to the formulations. The authors' findings suggest that, for recycled PP and without compatibilizers, there is an apparent upper limit (i.e., close to 5 wt%) of BF content that effectively reinforces the composite. However, injection molding processing showed that up to 40 wt% BF can be used as a filler in BF-PP composites by including a compatibilizer. 42 Therefore, further work is required to assess (a) the possibilities of using larger percentages of BF in the 3D-printed composite using neat PP, and (b) if larger percentages of BF limit the

mechanical properties of the 3D-printed BF-PP composites. The objective of this work is to fulfill these necessities and evaluate the performance of PP-BF composites produced via 3D printing, with no added compatibilizers, and understand the influence of adding varying proportions of BF on the composites' properties. To this end, PP was compounded with different percentages of BF (from 15 wt% to 45 wt%), and filaments were manufactured prior to 3D printing of specimens as required for mechanical testing. Tests were conducted to understand the rheological behavior of the formulations, visualize the morphology of the filaments, identify the thermal stability of the BF-PP formulations, and study the interaction between BF and PP. Mechanical tests were conducted to evaluate the mechanical performance of the different formulations.

2 MATERIALS AND METHODS

Polypropylene (PP) copolymer pellets (natural color), with a melt flow rate at 230°C/2.16 kg of 2.6 g/min and density of 0.89 g/cm³, were obtained from RheTech (Whitmore Lake, MI). Basalt fiber (BF) with dimensions 3 mm (long) \times 13 µm (diameter) and a density of 2.75 g/cm³ with silane sizing for PP resin was obtained from Sudaglass Fiber Technology, Inc (Houston, TX). Five formulations were prepared and tested: Neat PP, 15 wt% BF with 85 wt % PP, 25 wt% BF with 75 wt% PP, 35 wt% BF with 65 wt% PP, and 45 wt% BF with 55 wt% PP. These formulations are herein referred to as OBF100PP, 15BF85PP, 25BF75PP, 35BF65PP, and 45BF55PP, respectively. The selection of these percentages was based on previous works using other processes for manufacturing BF-PP composites. Deng et al. employed an injection molding process and added up to 40 wt% of BF in the composites, 42 and Saleem et al. used up to 50 wt% of BF in compression-molded BF-PP composites. 43 Thus, a comparison of properties is expected if the filler content is in the range of these values.

2.1 Filament production

After preparing the formulations (approximately 300 g in each case), three steps were followed for filaments production: (1) the corresponding formulation was compounded using a twin-screw extruder (Leistritz D90459 Type ZSE18HP-400) that possesses eight heating zones. The working temperature was 180°C in all heating zones and for all formulations. The screw rotation was set to 40 rpm. A cylindrical twin die (2.5 mm diameter) was used in this step. No forced cooling of the resulting filament was employed; (2) the extruded filament was then pelletized (C.W. Brabender Instruments, Inc Type: 12-74-000) to a

length of approximately 3-5 mm; and (3) the pellets were used for final filaments production using a capillary rheometer (Rheometer Scientific Acer 2000). In this step, two cylindrical dies were employed in the capillary rheometer, depending on the formulation, as indicated in Table 1, because not all formulations behaved the same way. Thus, different conditions for filament production were required (Table 1) to guarantee a filament diameter of approximately 1.75 mm, as required for the 3D printing process. The working schedule in the capillary rheometer was: (1) preheat the rheometer at the set temperature, (2) load the material in the rheometer's cylinder and hold for 10 min (to guarantee complete PP melting), (3) pre-pack until 180 mm at 2000 1/s, (4) soak (hold) at 180 mm for 1 min; and, (4) extrude the material from 180 to 320 mm at 2000 1/s or 2500 1/s, depending on the formulation (Table 1). Neat PP presented difficulties for filament production due to slow cooling; thus, compressed air was used to help cool down this material (no forced cooling was employed for the BF-PP formulations). The filaments were collected while continuously measuring the diameters and visually inspecting homogeneity and surface smoothness. The composite filament production in the rheometer was relatively easy, especially for the formulations with higher BF content. Up to 10 m of each filament was obtained for each formulation (See pictures in Figure 1).

2.2 Filaments testing

The filaments used for 3D printing were tested to determine: (a) the BF length distribution in the filament prior to 3D printing (i.e., after the extrusion + pelletizing process, since final filament production in the capillary rheometer does not affect fibers' length), (b) the effect of the amount of BF on the rheological behavior of the BF-PP formulations, and (c) surface morphology and circularity of the cross-section.

2.3 Fiber length distribution

For measuring the BF length distribution in the filaments, a portion of filaments from each formulation (approximately 4-5 g, in duplicates) was burnt using a convection furnace (Isotemp® muffle furnace Fisher Scientific) at 550°C for 10 min to remove PP. Then, particle size analysis of the basalt fibers (i.e., length distribution analysis) was carried out on the unburnt material. The test used a Malvern Mastersizer 300 equipment coupled to a Hydro LV Malvern wet dispersion unit working at 2400 rpm. For the test, approximately 200 mg of the BF obtained after the burning process was added to distilled water in

Formulation	Die	Working temperature	Sweep rate
0BF100PP 15BF85PP 25BF75PP	$2.5 \text{ mm} \times 30 \text{ mm}^{a}$	185°C	2500 1/s
35BF65PP 45BF55PP	2.0 mm × 30 mm	190°C	2000 1/s

^aInternal diameter × length.





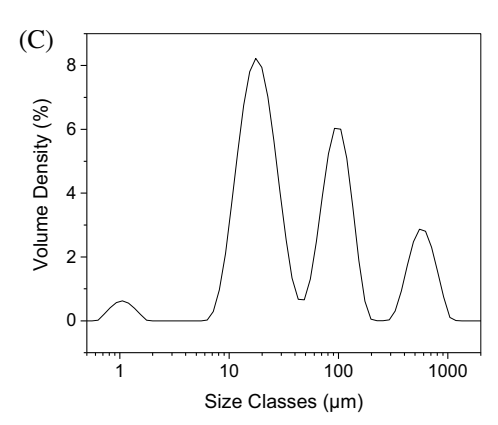


FIGURE 1 (A) Picture of the 15BF85PP formulation filament, (B) Picture of the filaments of the other BF-PP formulations, (C) Typical particle size distribution of BF in the filaments (regardless of BF content).

the equipment's dispersion unit to reach an obscuration of \sim 14%. The ultrasound option was turned on (at 70% level) during the tests. Five measurements were carried out for each formulation.

2.4 | Rheological behavior

Rheology tests were conducted using parallel plates and capillary rheometers.

2.4.1 | Parallel plate rheology

Parallel plate rheology of the BF-PP formulations, using a disc-size specimen produced with pellets from the filaments, was conducted on a TA Instruments DHR-2 rheometer. Pellets cut from filament were poured into a 5'' by 5'' (125 mm \times 125 mm) mold cavity with 1 mm thickness and hot pressed using a $6'' \times 6''$ (150 mm \times 150 mm) Carver Hydraulic Mold Press to generate a thin film. Pellets were pressed at 185°C for 5 min by applying 27.57 MPa of pressure. The thin film was then cut into a disc shape using a hole saw cutter. The parallel plate specimen with a diameter of 20 mm and a gap of 1 mm was adopted. The five formulations were tested in oscillation amplitude mode under continuous oscillation in the 0.01 to 100 1/s shear rate at

185°C. The specimen was placed on the lower heated plate in the rheometer, and the moveable plate was lowered to hover above the disc to melt it for approximately one minute.

2.4.2 | Capillary rheology

The capillary rheometer test was intended to better assess the formulations' behavior at shear rates higher than those used in the parallel plate rheometer. Rheology tests using capillary rheology better replicate the behavior of the materials under the conditions used in industrial processing⁴⁴ (i.e., relatively high shear rates). Capillary rheology tests were conducted on the Acer 2000 equipment employed for filament production. Approximately 80 g of each formulation (in duplicates) were used for the tests. As in the work of Rhodes et al.,45 a die with L/D = 20 (i.e., 30 mm long and 1.5 mm internal diameter) was used for all tests. $L/D \ge 20$ has been recommended for capillary rheology tests of viscous materials.⁴⁴ The testing temperature was 220°C, that is, the same used for 3D printing (See Section 2.3). After loading, the materials were allowed to melt and reach thermal equilibrium for around ten minutes before the measurements. The sequence in the equipment was: (1) prepacking to length 220 mm at 2000 1/s, (2) presoak

for 60 s, and (3) testing (measuring) at ten specified shear rates (i.e., 2000, 1000, 800, 400, 200, 100, 80, 40, 20, 10 1/s). The steady-state time for each shear rate was 60 s, which was sufficient to obtain constant stress versus time curves (a required condition for data point collection) before moving to the next selected shear rate.

SEM of filaments 2.5

Scanning electron microscopy (SEM) was employed to visualize the surface morphology (smoothness) and the circularity of the filaments' cross-section. The SEM test was conducted using Tescan SEM equipment working at 20 kV after gold sputtering.

2.6 3D printing

For each formulation, up to eight Type V tensile testing coupons (length overall of 63.5 mm, width overall of 9.53 mm, and thickness of 3.2 mm, as per ASTM D638) were 3D printed employing an ANYCUBE i3 Mega 3D printer (at room temperature), using a hardened steel nozzle (0.6 mm diameter) to minimize abrasion of BF on nozzle's internal surfaces. The extruder temperature was set to 220°C, and the plate temperature was 90°C in all cases. For adequate adhesion of the 3D printed specimens, the plate was covered with 3M Scotch® Super-hold adhesive tape (which is a PP-based tape). Other parameters used were: infill density of 25% (a typical value in 3D printing works as mentioned, for example, in Coughlin et al.⁴¹), layer cooling fan was ON (at 100% capacity); zigzag infill pattern (45°); wall thickness of 1.2 mm (i.e., double the diameter of the die exit); layer height of 0.2 mm; and, a print speed of 30 mm/s. Print cooling was enabled at 100%. In addition to the tensile coupons, five specimens for Izod Pendulum Impact (length of 63.5 mm, width of 12.7 mm, and thickness of 3 mm, following ASTM D256) were produced for each formulation (except for neat PP, from which only three specimens were produced due to the difficulty of 3D-printing this material and extreme warping and lack of enough filament of neat PP after filament production), using the same parameters employed for the tensile testing coupons. Welding of the first deposited layer onto the build platform (i.e., scotch tape) was observed in some samples after removing the 3D-printed specimens. We also observed that even using the adhesive tape on the plate, obtaining dimensionally accurate 3-D printed samples of neat PP was challenging, which explains why only a few specimens were successfully 3-D printed. The apparent density of the final specimens was determined by weighing the 3D-printed

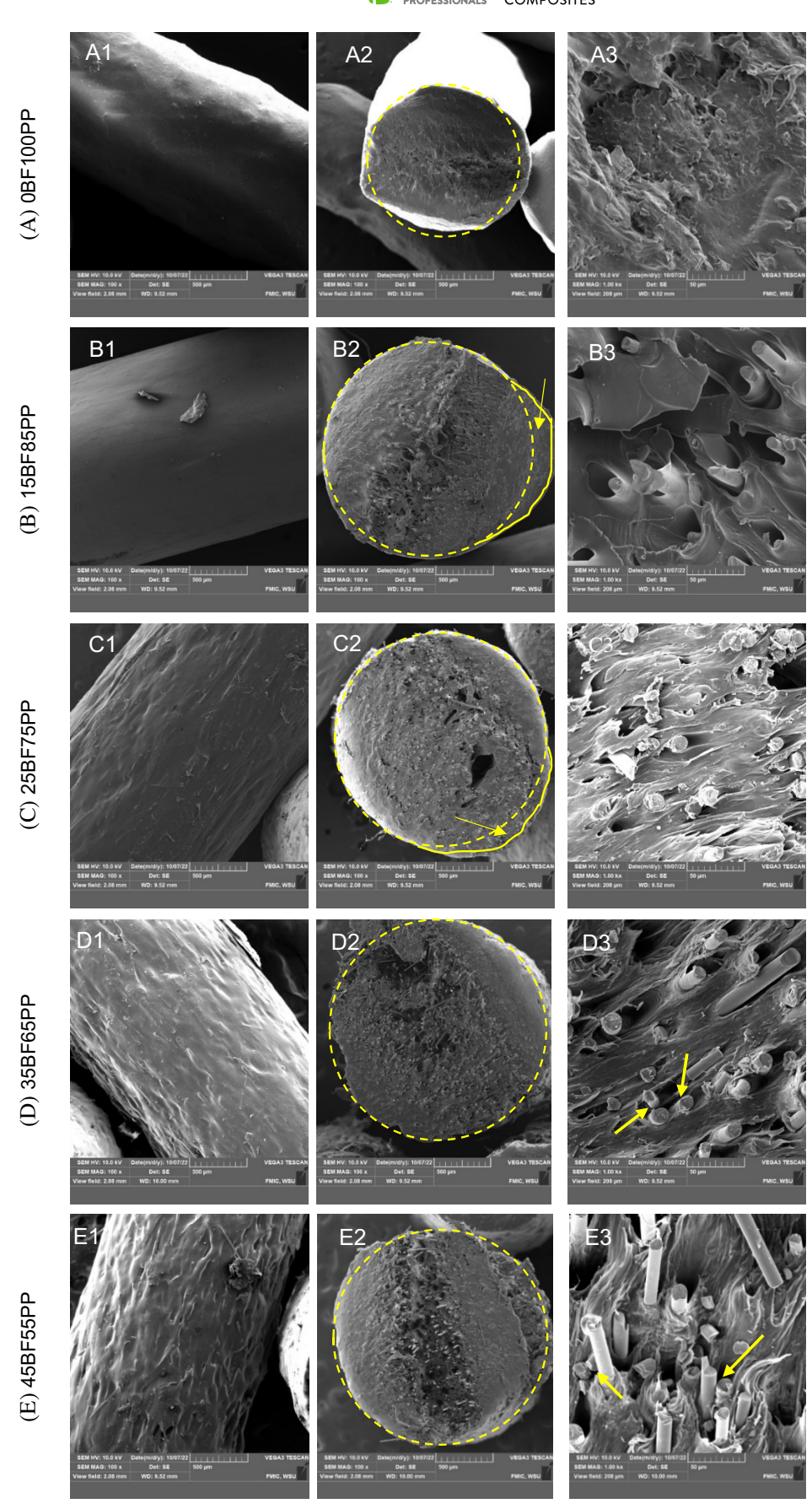
specimens and calculating the corresponding volume (using SolidWorks). The total time for 3D printing tensile and impact specimens was \sim 19 min and \sim 30 min, respectively. Furthermore, additional specimens were 3D printed for formulations 35BF65PP and 45BF55PP using 50% and 100% infill density (keeping the other parameters employed for the 25% infill specimens) to find the effect of infill density on tensile strength and Izod impact resistance.

Testing of 3D printed specimens 2.7

Tensile tests of the V-type coupons were conducted following ASTM D638 using an Instron (Model 4466) universal testing machine. Five specimens obtained via 3D printing (Section 2.6) were directly tested under tensile conditions using an Epsilon extensometer with a gauge length of 12.5 mm (Model 3442-0050-010-ST) to record the displacement. The testing speed was 1 mm/min. Wedge-action tensile grips were used for the tests. Izod pendulum impact tests of the 3D printed specimens were carried out at room temperature following ASTM D256, using a Dynisco BPI (Basic Pendulum Impact Tester) equipment. Prior to the test, the specimens were separately notched at room temperature as per the ASTM D256 standard. Four specimens of each formulation were employed in the tests, except for the 0BF100PP formulation (from which only two specimens were tested, due to the difficulty of obtaining flat 3D-printed prismatic specimens). Analysis of variance (ANOVA) using OriginPro 2017 (Northhampton, MA, USA), with confidence level $\alpha = 0.05$, was conducted to determine the statistical significance of the results.

Thermogravimetric analysis (TGA) was carried out to (a) investigate the effect of adding BF on the thermal degradation of the composites and (b) assess if the BF content in the composite is close to the target BF content throughout the 3D printed tensile coupons. For the test, samples (25% infill density) were randomly taken from the tested tensile coupons (i.e., after the compounding and 3D-printing process) and subjected to TGA using a Mettler Toledo TGA/DSC 1 equipment at a heating rate of 10°C/min, from room temperature to 600°C, with nitrogen as carrier gas. Differential Scanning Calorimetry (DSC) was used to determine the thermal stability of the 3D-printed composites. The test was conducted on a STARe System DSC 1 (Mettler Toledo, Columbus, OH) with Mettler Toledo STARe Evaluation Software 16.40. The neat PP and the four BF-PP formulations were heated, cooled, and heated again using a heating/cooling rate of 10°C/min in the range of temperatures from 20 to 200°C and nitrogen as carrier gas. Scanning electron microscopy (SEM) was employed to observe fiber/matrix

FIGURE 2 SEM pictures of the surfaces (column 1) and the cross sections (columns 2 and 3) of the filaments of (A) Raw PP (i.e., 0BF100PP), (B)15BF85PP, (C) 25BF75PP, (D) 35BF65PP, and (E) 45BF55PP formulations.



interfacial bonding in the 3D printed specimens after the tensile tests, following the same procedure for testing the filaments.

3 RESULTS AND DISCUSSION

Figure 1A,B show pictures of filaments used for 3D printing obtained from the capillary rheometer. The final diameters of the filaments were 1.67 ± 0.09 , 1.69 ± 0.10 , 1.74 ± 0.06 , 1.75 ± 0.06 , and 1.74 ± 0.03 mm for the 0BF100PP, 15BF85PP, 25BF75PP, 35BF65PP, and 45BF55PP formulations, respectively (means of diameters at ten different randomly selected filaments' lengths). As expected, the production of the neat PP filament was challenging because the material was prone to shrinking, that is, reducing its diameter when cooling (See also Section 3.5). The addition of BF reduced this PP's tendency, and the target diameter (i.e., approximately 1.75 mm) was more easily achieved, especially for formulations containing 25 wt% BF and above. Also, as seen in the pictures (Figure 1), the resulting filaments are very flexible, which contrasts with the preparation of filaments using other types of fillers, such as GF, in which some degree of brittleness has been identified.²⁸

A typical BF particle size distribution of the fibers, regardless of the BF content in the composite, is shown in Figure 1C. The BFs of the BF-PP filaments are constituted mainly by short fibers with lengths below 1000 µm, with approximately half the fibers' length ranging from 7 to 50 µm. The standard percentile readings from the analysis for each formulation, as reported by the Mastersizer equipment, were: $Dv10 = 11.80 \pm 0.04 \mu m$; $Dv50 = 28.40 \pm 0.04 \mu m$ $0.15 \mu \text{m}$; and $Dv90 = 476 \pm 8.98 \mu \text{m}$ (where, for example, the Dv90 category represents the size of the particle below which 90% of the sample lies). The reduction of particle size compared to the raw BFs results from the compounding process in the extruder. Interestingly, the length of the BF fibers in the composites is close to the length of GF used by Shulga et al.,27 who manufactured GF-reinforced PP 3D printed composites.

3.1 Morphology of filaments

Figure 2 shows SEM images of the filaments of each formulation. Filaments' surface smoothness was excellent for 0BF100PP, 15BF85PP, and 25BF75PP formulations (Figure 2A1-C1, respectively) despite the lack of compatibilizers in the formulations. The better surface morphology among all formulations corresponds to the 15BF85PP formulation. The 35BF65PP and the 45BF55PP filaments show higher surface roughness (Figure 2D1-E1) due to higher amounts of BF. A filament with a smooth surface

is a positive feature for 3D printing applications.³⁰ SEM images of the cross-section of the filaments (Figure 2A2-E2) show the circularity of the filaments' cross-section. A yellow circle has been drawn in the micrographs for comparison purposes. Figure 2A2 exhibits a shrinking behavior of PP. A slight deviation from circularity (as highlighted with a yellow line in Figure 2B2 and 2C2) can be observed for 15BFPP and 25BFPP formulations. The cross-sections of the 35BF65PP and 45BF55PP filaments are closer to the expected circular shape.

The right column of Figure 2 presents magnified SEM pictures of the cross-section of the filaments. In all cases, it is seen that the BF fibers are aligned with the longitudinal direction of the filaments. In the 15BF85PP and 25BF75PP formulations, excellent fiber dispersion is identified, and no fiber aggregations are observed (i.e., the fibers are isolated from each other and completely covered by a PP layer). However, the 35BF65PP and 45BF55PP formulations show that some fibers are not isolated from each other, and agglomerations of fibers exist. Detachment in the surface between BF and PP and shorter distances among BF are also identified (see the yellow arrows in the micrographs). These findings result from the high amounts of BF in these two formulations.

3.2 Rheological behavior

Results on the rheological tests of the formulations employed for 3D printing using the parallel plate rheometer (Figure 3) show that all BF-PP formulations present a classical behavior of filled polymers. The complex viscosity (η^*) of neat PP at the lower ω (up to ~ 1 1/s) is relatively constant and decreases at higher angular frequencies (Figure 3A), as expected for neat PP. 46 The addition of BF in all formulations increases η^* , indicating that the filler requires longer relaxation time to flow. As expected, the complex viscosity increases with BF content, regardless of the frequency, showing the filling effect of BF. In the 45BF55PP composite, yield stress occurs, indicating lower warpage when filler content increases. Shear thinning behavior was also observed in all curves as the shear rate increased. Thus, in all formulations, the complex viscosity decreases as the frequency increases, suggesting that the materials become less viscose at higher frequencies. These results are confirmed by the rheological behavior of the composites using the capillary rheometer (Figure 4). The results of the capillary rheology show relatively large differences among the values of complex viscosities at the lowest shear rate (i.e., 10 1/s). The measured complex viscosities are 254, 282, 370, 418, and 591 Pa.s for the 0BF100PP, 15BF85PP, 25BF75PP, 35BF65PP, and 45BF55PP formulations, respectively. Yet, the lower resistance to flow under

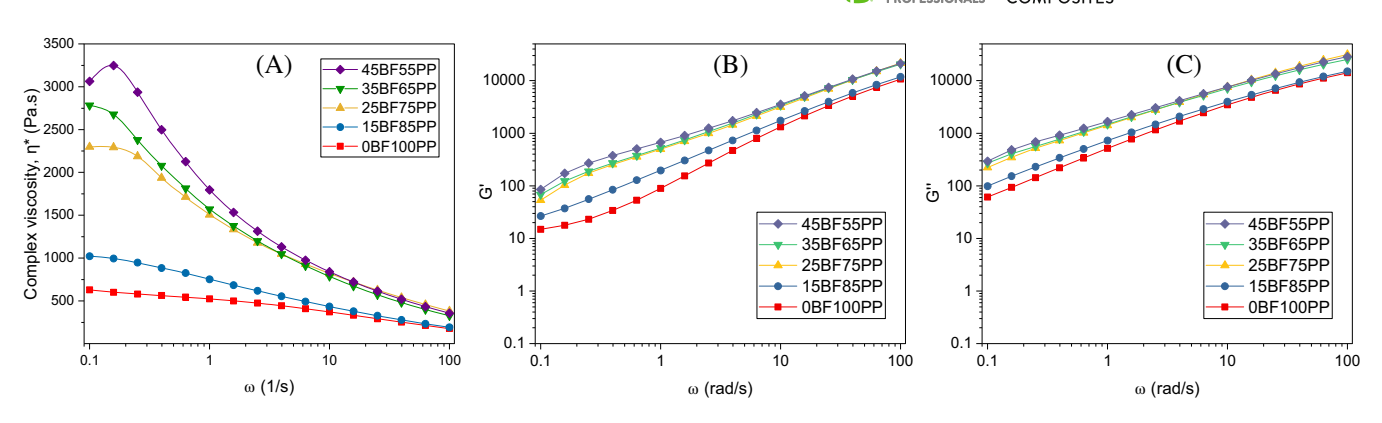


FIGURE 3 Parallel plate rheology curves of (A) η versus frequency (ω), (B) G' versus ω , and (C) G" versus ω of the formulations (0BF100PP, 15BF85PP, 25BF75PP, 35BF65PP, and 45BF55PP) used for 3D printing.

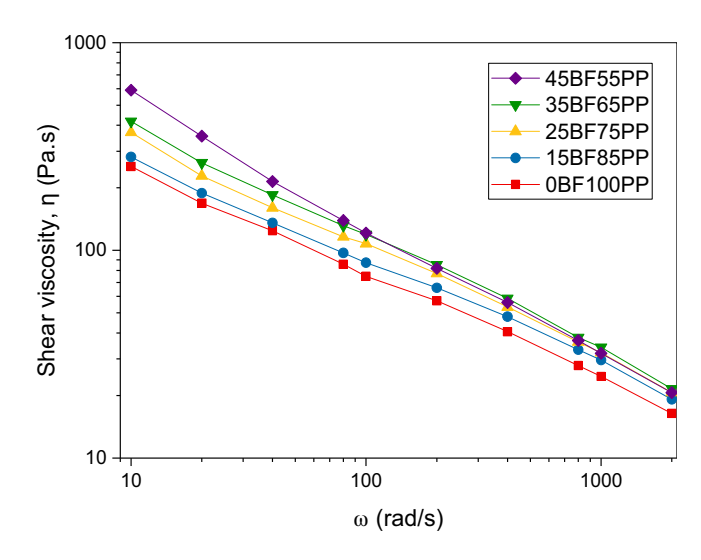


FIGURE 4 Curves of shear viscosity versus shear rate (ω) of the formulations used for 3D printing (capillary rheometer).

high shear rates is expected to positively impact the 3D printing of the formulations because the rheology of the composite is dominated by the rheology of the matrix. When processed at high shear rates (i.e., above 100 1/s), all composites show approximately similar behavior. Potential issues such as nozzle clogging or reduced extrudability were not identified in the process.

Based on the η versus ω results shown in Figure 3A, two groups of BF-PP composites can be distinguished: (1) 0BF100PP and 15BF85PP, and (2) 25BF75PP, 35BF65PP, and 45BF55PP formulations. The formulations of each group have close complex viscosities at high shear rates. Approximately similar complex viscosity at high shear rates indicates that all formulations should work similarly when processed to produce composites using FDM since polymer processing usually involves high share rates. The 15BF85PP formulation can also require less energy for processing than the 25BF75PP, 35BF65PP, and 45BF55PP formulations. The rheological

behavior of the composites also has implications for the printability of the formulations. According to Schwab et al.,⁴⁷ "the concept of printability assessment for extrusion printing includes rheological characterization, extrudability, and filament formation as well as shape fidelity"; thus, the rheological properties largely influence composites' printability. Therefore, all formulations, when processed at high shear rates (i.e., above 100 1/s), are expected to possess approximately similar printability.

Figure 3B,C show that both the storage modulus (G') and the loss modulus (G") of all formulations (in the parallel plate rheometer) decrease as the frequency decreases. Improvement of G' is due to the presence of the filler, which partially restricts the movement of the PP chains. 46 It is also seen that, in the entire ω region tested, G" is higher than G'. suggesting that all formulations behave like viscous materials. Moreover, a visible increase of both G' and G" occurs as the BF content increases in the formulations. Higher G" indicates the composites' ability to dissipate energy as heat when subjected to cyclic or dynamic loading due to the filler's additional interfaces, irregularities, and interactions within the composite. The G' increase can be explained because higher filler concentrations and well-aligned filler networks can increase the composite's reinforcing effect and stiffness.

3.3 | DSC results

Figure 5 shows the DSC curves corresponding to the first cooling and second heating and Table 2 shows the scanning calorimetric data obtained for the BF-PP formulations. It is observed that the percentage of crystallinity (X_c) decreases in the formulations with lower loading levels of BF (i.e., 15 and 25 wt% of BF) while T_c and T_m increase compared with net PP. This probably results from the PP crystallite size (the size of the spherulites) within the composite matrix. Well-dispersed short fillers

15480569, 2024, 13, Downloaded from https://4spepublications

onlinelibrary.wiley.com/doi/10.1002/pc.28641 by Readcube (Labtiva Inc.), Wiley Online Library on [28/01/2025]. See the Terms and Conditions (https://original.com/doi/10.1002/pc.28641 by Readcube (Labtiva Inc.), Wiley Online Library on [28/01/2025]. See the Terms and Conditions (https://original.com/doi/10.1002/pc.28641 by Readcube (Labtiva Inc.), Wiley Online Library on [28/01/2025]. See the Terms and Conditions (https://original.com/doi/10.1002/pc.28641 by Readcube (Labtiva Inc.), Wiley Online Library on [28/01/2025]. See the Terms and Conditions (https://original.com/doi/10.1002/pc.28641 by Readcube (Labtiva Inc.), Wiley Online Library on [28/01/2025]. See the Terms and Conditions (https://original.com/doi/10.1002/pc.28641 by Readcube (Labtiva Inc.), Wiley Online Library on [28/01/2025]. See the Terms and Conditions (https://original.com/doi/10.1002/pc.28641 by Readcube (Labtiva Inc.), Wiley Online Library on [28/01/2025]. See the Terms and Conditions (https://original.com/doi/10.1002/pc.28641 by Readcube (Labtiva Inc.), Wiley Online Library on [28/01/2025]. See the Terms and Conditions (https://original.com/doi/10.1002/pc.28641 by Readcube (Labtiva Inc.), Wiley Online Library on [28/01/2025]. See the Terms and Conditions (https://original.com/doi/10.1002/pc.28641 by Readcube (Labtiva Inc.), Wiley Online Library on [28/01/2025]. See the Terms and Conditions (https://original.com/doi/10.1002/pc.28641 by Readcube (Labtiva Inc.), Wiley Online Library on [28/01/2025]. See the Terms and Conditions (https://original.com/doi/10.1002/pc.28641 by Readcube (https://original.com/doi/10.10

ions) on Wiley Online Library for rules of use; OA articles are governed by the applicable Creative Commons License

(B) Second Heating

0BF100PP

15BF85PP 25BF75PP 35BF75PP 45BF55PP

120

100

80

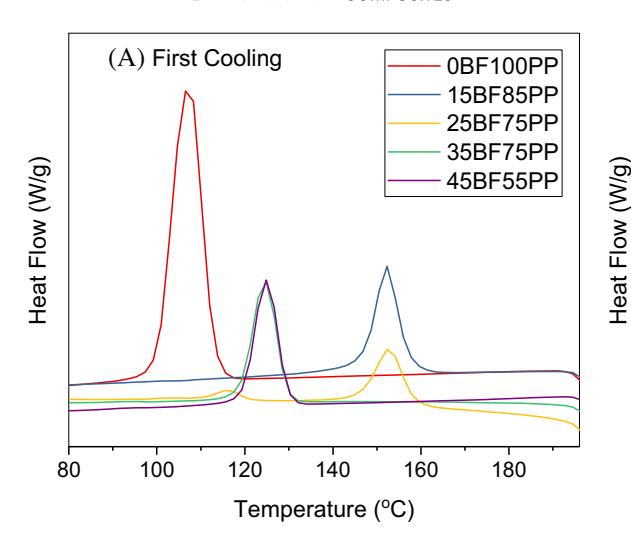


FIGURE 5 Curves corresponding to the DSC (A) first cooling and (B) second heating of BF-PP composites.

TABLE 2 Scanning calorimetry data corresponding to the different formulations.

Formulation	T _c (°C)	T_m (°C)	$\Delta H_{m} (J g^{-1})$	X_c
0BF100PP	108.2	166.9	101	49
15BF-85PP	152.7	192.9	26	15
25BF-78PP	153.1	194.6	29	19
35BF-65PP	125.0	165.5	60	45
45BF-55PP	125.3	165.6	56	49

can act as nucleating agents, increasing the length of the polymer folding to form crystals and consequently requiring more energy for the polymer to melt. 48 It possible that fewer but larger crystals are formed at low BF concentrations since the dispersed fibers can be more effectively coated with a PP layer (See Figure 2) than in formulations with higher BF content. Thus, 15 to 25 wt% of BF could be more easily integrated into the PP matrix, providing a more favorable environment for crystals to grow. Meanwhile, in the formulations containing 35% and 45% BF, the percentage of crystallinity (X_c) and T_m remains similar to that of neat PP, while T_c increases. This suggests that, at higher filler content, more energy is required to initiate the crystallization process since the filler can introduce unwanted effects, such as filler-filler agglomeration, decreased chain mobility, BF-BF interactions, limited space for the matrix amid BFs, and detachment between BF and PP at the interface.

3.4 TGA results of 3D printed composites

The TGA curves (Figure 6A) show the influence of BF on the thermal stability of PP. For all the BF-PP formulations (i.e., regardless of the filler content), \sim 5% of weight loss occurs at around 415°C. The initial degradation temperature is approximately similar for all formulations, with a variation of a few Celsius degrees only. The maximum rate of change of mass with respect to time (i.e., maximum in the DTG curve in Figure 6B) corresponding to each formulation shifts from 459.6°C for pure PP to 468.3°C for the 45BF55PP formulation. Thus, the BF in the composites increases the thermal stability of the composite compared to neat PP, probably because of the BF's higher thermal stability than PP's (i.e., BF's thermal expansion coefficient can be \sim 8 to 10 times lower than PP's. See Section 3.5), which is limiting the heat transfer to PP to start degrading. The TGA curves also serve to confirm that the BF content in the 3D-printed composites is approximately similar to the target BF content for each formulation. Specifically, the BF contents are 15.0, 22.9, 33.1, and 42.1 wt%, for the 15BF85PP, 25BF75PP, 35BF65PP, and 45BF55PP formulations, respectively, corresponding to the undegraded material after 500°C. These results suggest that the procedure used in the work ensures that the BF content is close to the target content.

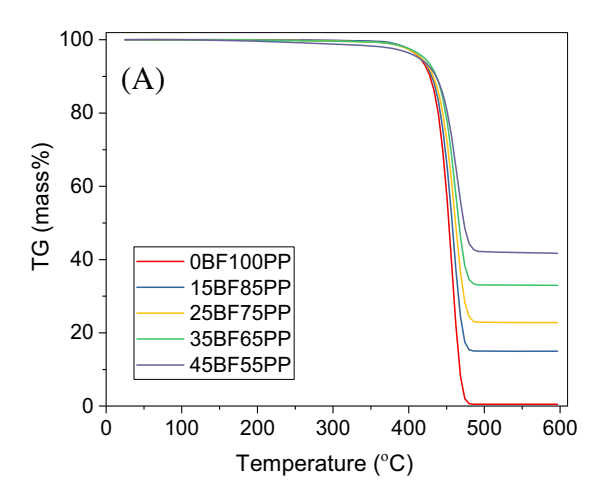
3.5 | Mechanical properties of the 3D printed composites

Examples of typical stress-strain curves of the tested composites are presented in Figure 7, showing that the strain of the composites is largely decreased when compared to neat PP. Pictures of the specimens used for the tensile tests and the Young's moduli corresponding to each formulation are summarized in Table 3. The results show that the increase in Young's modulus (E) of the composite material is statistically significant (at the $\alpha = 0.05$ level; in the table,

15480569, 2024, 13, Downloaded from https://4spepublicati

onlinelibrary.wiley.com/doi/10.1002/pc.28641 by Readcube (Labtiva Inc.), Wiley Online Library on [28/01/2025]. See the Terms and Conditions (https://originals.com/doi/10.1002/pc.28641 by Readcube (Labtiva Inc.), Wiley Online Library on [28/01/2025]. See the Terms and Conditions (https://originals.com/doi/10.1002/pc.28641 by Readcube (Labtiva Inc.), Wiley Online Library on [28/01/2025]. See the Terms and Conditions (https://originals.com/doi/10.1002/pc.28641 by Readcube (Labtiva Inc.), Wiley Online Library on [28/01/2025]. See the Terms and Conditions (https://originals.com/doi/10.1002/pc.28641 by Readcube (Labtiva Inc.), Wiley Online Library on [28/01/2025]. See the Terms and Conditions (https://originals.com/doi/10.1002/pc.28641 by Readcube (Labtiva Inc.), Wiley Online Library on [28/01/2025]. See the Terms and Conditions (https://originals.com/doi/10.1002/pc.28641 by Readcube (Labtiva Inc.), Wiley Online Library on [28/01/2025]. See the Terms and Conditions (https://originals.com/doi/10.1002/pc.28641 by Readcube (Labtiva Inc.), Wiley Online Library on [28/01/2025]. See the Terms and Condition (https://originals.com/doi/10.1002/pc.28641 by Readcube (Labtiva Inc.), Wiley Online Library on [28/01/2025]. See the Terms and Condition (https://originals.com/doi/10.1002/pc.28641 by Readcube (Labtiva Inc.), Wiley Online Library on [28/01/2025]. See the Terms and Condition (https://originals.com/doi/10.1002/pc.28641 by Readcube (Labtiva Inc.), Wiley Online Library on [28/01/2025]. See the Terms and Condition (https://originals.com/doi/10.1002/pc.28641 by Readcube (https://origina

nditions) on Wiley Online Library for rules of use; OA articles are governed by the applicable Creative Commons



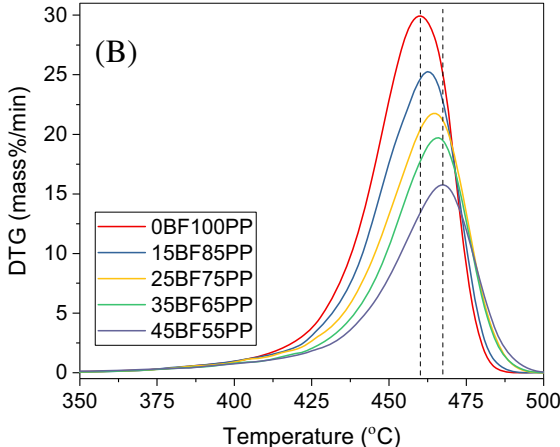


FIGURE 6 Examples of: (A) TGA and (B) DTG curves of the 3D printed composites.

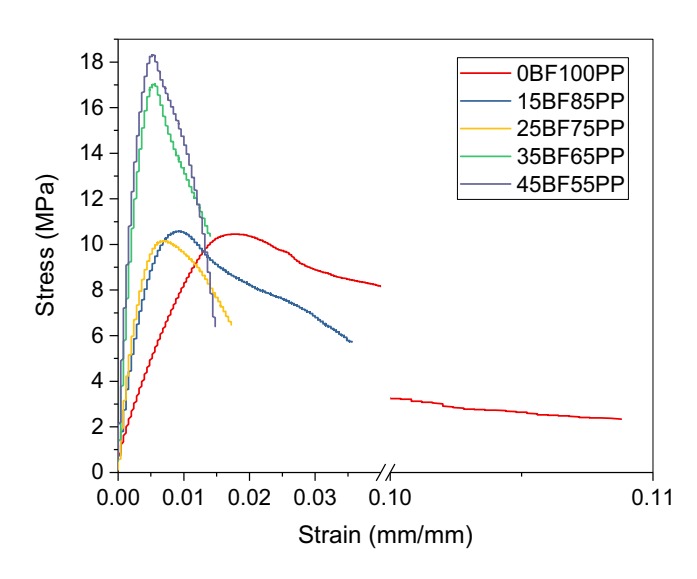


FIGURE 7 Typical stress-strain curves for the BF-PP composites tested (Note the break from 0.04 to 0.1 mm/mm in the x-axis to better show the whole curve for neat PP).

values with same letters are not significantly different) when the BF content is increased, except when BF is increased from 35 to 45 wt%, at which point the difference is not statistically significant. These results confirm the expected reinforcing effect of BF in the composites. The apparent density of the 0BF100PP specimen is below that of the neat PP (i.e., 0.890 g/cm³). This result is expected because of the low infill density of the specimens (i.e., 25 wt%). Likewise, the densities of the other formulations are lower than that of neat PP, also because of the low infill density, except for the 45BF55PP formulation (due to the large amount of BF). The E of 3D-printed neat PP (1.08 GPa) is higher than previously reported values for PP. Stoof et al.5 reported Young's modulus of neat 3D-printed PP of 0.892 GPa, and Yang et al.

reported E of 0.773 ± 0.012 GPa.⁴⁹ For comparison purposes, the E of the 3D-printed BF-PP composites herein (~4.2 GPa for the formulations with amounts of BF greater than 35%, as seen in Table 3) is approximately 55% the E of injectionmolded BF-PP composites containing 40 wt% of BF, with 2 wt% MAPP as a compatibilizer (i.e., 7.73 ± 0.73 GPa). 42 The lower values of E in the 3D-printed BF-PP composites are due to the low infill density.

Table 3 shows that the Young's moduli of the 3D printed composites are higher than that of PP in all cases, which is expected as the presence of the filler reinforces the composites. However, a significant increase in Young's modulus is achieved when the proportion of BF increases in the formulation (above 35% in this study). The E of 35BF65PP and 45BF55PP is approximately similar (~4.25 GPa) and approximately four times higher than that of neat 3D-printed PP. The E of these formulations is also higher than values reported for PP-based 3D printed composites containing 30% harakeke, using a compatibilizer (MAPP) (i.e., ~2.70 GPa). One possible reason for the relatively higher E in the BF-PP composites is because of the large amounts of BFs, as the E for BF filaments is around 89 GPa, according to the supplier. Regarding the UTS, results in Table 3 show that, statistically, there are differences among the values corresponding to each formulation. A decrease in UTS is observed in formulations with 15 and 25 wt% of BF when compared to neat PP, but UTS is higher than in neat PP in the formulations with 35 and 45 wt% of BF. These results indicate that significant amount of BF fiber is required in a formulation to achieve adequate interaction between the sized BF and PP to improve the strength of a 3D printed composite material (as indicated by the stress-strain behavior in Figure 7). Moreover, results also indicate that sizing of BF could be improved significantly to yield higher composite strength.

TABLE 3 Results of mechanical tests of BF-PP composites (25% infill density).

Formulation	Specimen's picture	Apparent density (g/cm³)	Young's Modulus ^a (GPa)	E relative increase (%) ^b	UTS ^a (MPa)
0BF100PP		0.582 ± 0.046	$1.08 \pm 0.09 (A)$	-	$14.76 \pm 2.64 (A)$
15BF85PP		0.588 ± 0.011	1.42 ± 0.21 (B)	31.3	10.73 ± 0.43 (B)
25BF75PP		0.606 ± 0.012	1.80 ± 0.09 (C)	73.9	8.95 ± 1.07 (C)
35BF65PP		0.876 ± 0.022	$4.24 \pm 0.29 (D)$	291.9	$18.07 \pm 0.84 (D)$
45BF55PP		0.940 ± 0.020	$4.25 \pm 0.44 (D)$	292.5	$17.67 \pm 0.91 (D)$

^aDifferent letters in parenthesis indicate statistically significant differences in values at the $\alpha = 0.05$ level.

^bPercent increase taking neat PP as a reference.

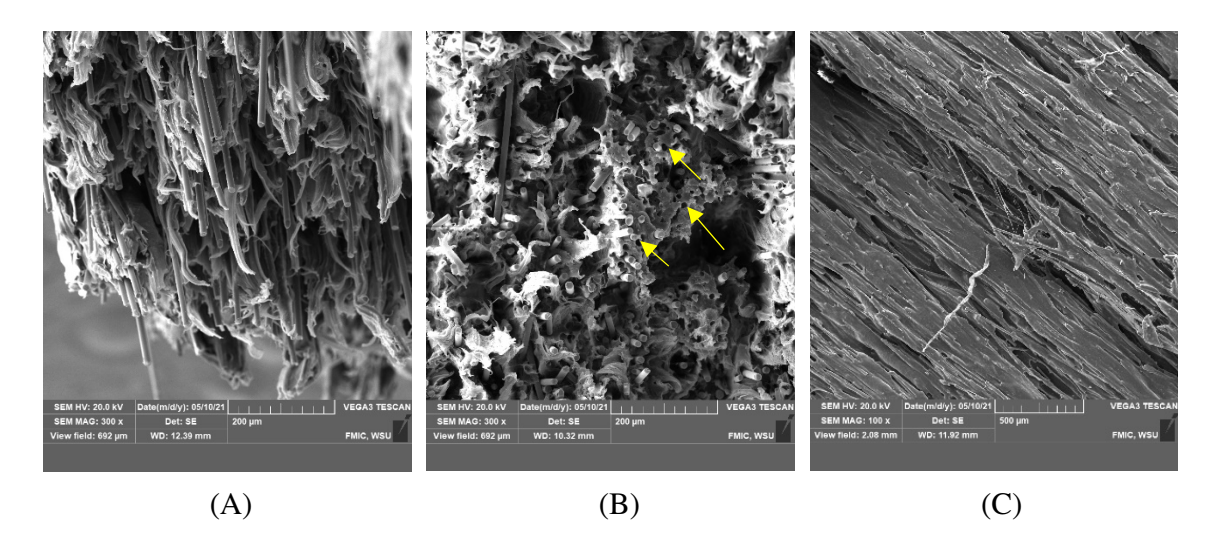


FIGURE 8 SEM pictures corresponding to the fracture of 3D-printed composites showing fiber's pullout after tensile tests of the 45BF55PP formulation (A, B) and BFs' alignment during 3D printing (C).

Figure 8 presents SEM micrographs corresponding to the fracture of the 3D-printed composites after the tensile tests. Figure 8A shows no damage or breakage of the BFs after the tensile tests, indicating that the fracture is mainly due to matrix cracking and fiber pullout. This is confirmed by Figure 8B, where holes in the matrix (some of which are highlighted with yellow arrows) are visible post-tensile test due to fiber detachment. Moreover, the BFs' surfaces do not exhibit any adhered residue of PP after the tests (Figure 8A). These observations indicate relatively poor interface interaction between the fiber and the matrix. However, the adhesion appears sufficient to improve the mechanical properties of the composite (Table 3). Furthermore, it is known that the role of the fiber as reinforcement in the composite depends on the fiber distribution and orientation within the composite.³⁵ Good distribution of fibers and fiber alignment is observed in the 3D-printed BF-PP composites (Figure 8A,B), which is consistent with the 3D processing method, as confirmed by Figure 8C.

The improved mechanical performance for BF-PP composites compared to neat PP, as seen in Table 3, is

due to the reinforcing effect of BF within the matrix. This enhancement can be attributed to the existing BF-PP interface interaction, combined with other factors such as BF's mechanical properties and its appropriate distribution and orientation within the matrix.³⁵

Figure 9A shows pictures of the 3D printing specimens for the Izod impact tests. The pictures show that the visible warping of neat PP 3D printed specimens is avoided by introducing BF as a reinforcer (Figure 9B). Warping and shrinking of PP in 3D printing occurs because, as melt PP cools down, the volume (i.e., the free volume between the macromolecular chains and their vibrational volume) decreases as long as the material's temperature is above the glass transition temperature.³¹ The relatively high thermal expansion coefficient of PP (i.e., up to $\sim 62 \times 10^{-6} \text{ 1/°C}$ at 160°C)⁵⁰ makes PP expand in all directions when heated, causing the poor dimensional stability of the 3D printed PP specimen upon cooling. Meanwhile, the low thermal expansion coefficient of BF (8 \times 10⁻⁶ 1/K), which is close to that of GF (i.e., 5.4×10^{-6} 1/°C), 35 helps the 3D printed BF-PP composites to keep the shape and dimensional stability regardless of the BF percent.

FIGURE 9 (A) Comparison of the tendency to warping of 3D printed neat PP (white color) and BF-PP composites, (B) the tendency to warping of PP 3D printed specimens is drastically reduced by the addition of BF.

The tendency of PP to warp in 3D printing processes has been reported previously.^{28,31} Therefore, the addition of BF to PP for 3D printing has avoided the warpage (specifically, the cupping) that occurs in 3D printed neat PP. The addition of BF as a filler in the PP-based composite improves the dimensional accuracy of PP-based 3D-printed composites. Commercially available PP-based filaments do not report the use of BF for this purpose. Previous works have also shown 3D-printed composites using up to 40% BF in ABS-based composites. However, 3D printing of PP-based composites reinforced with lignocellulosic fibers above 30% presents limitations.⁵ Moreover, studies on PP-based 3D printed composites reinforced with GF usually have used up to 30% of GF. 2,28 Thus, high amounts of BF in BF-PP composites appear less challenging to 3D print than formulations containing other types of reinforcing fibers.

Regarding the Izod impact resistance, the break in all specimens was a hinge type, which agrees with previous findings. 45 Figure 10 shows that the neat PP yields statistically (at the $\alpha = 0.05$ level) higher impact resistance than the composite materials (except for the 15BF85PP formulation) since impact resistance is reduced as BF is added to the composite. Interestingly, there is no statistical difference in Izod impact resistance in formulations that contain 25, 35, and 45 wt% of BF. This finding suggests that the BFs do not have an energy shielding effect in the composite, probably due to poor BF-PP interfacial bonding that hinders the dissipation of energy received during impact. However, the impact resistance of the 3D printed PP-based composites (Figure 10) is higher than that of injection molded crystalline cellulose reinforced PP composites reported by Yang et al.,9 who showed impact strength of notched specimens of $8.88 \pm 0.73 \text{ kJ/m}^2$ for PP

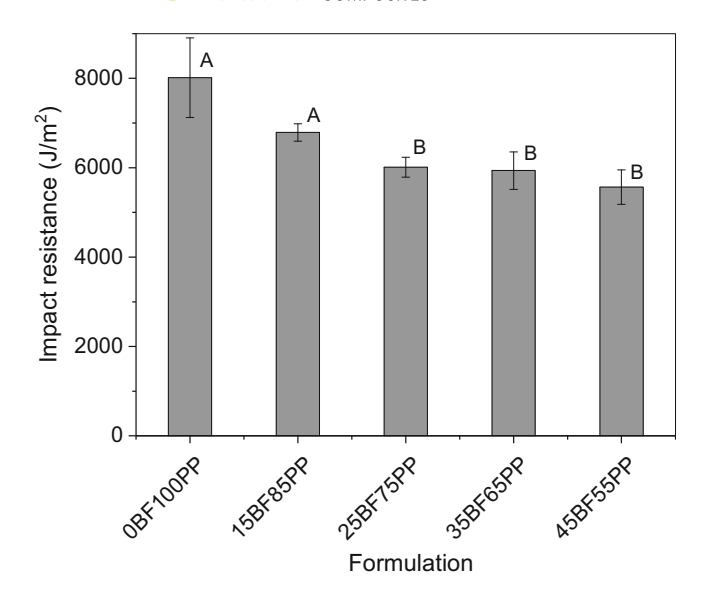


FIGURE 10 Izod impact resistance of BF/PP formulations. Bars with different letters indicate statistically significant differences at the $\alpha = 0.05$ level.

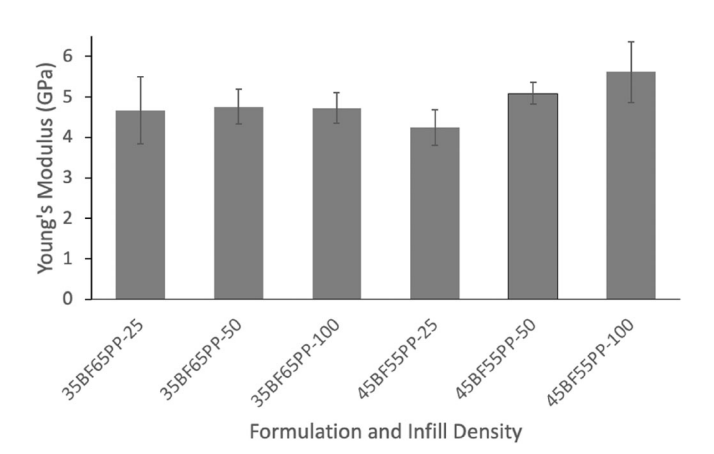


FIGURE 11 Effect on infill density on Young's Modulus (E) of 35BF65PP and 45BF55PP composites (the value after the dash shows infill density).

and up to $5.70 \pm 0.31 \text{ kJ/m}^2$ for composites reinforced with 1% microcrystalline cellulose. Moreover, the impact strength of all BF-PP formulations is comparable to values reported by Deng et al.⁴² for injection molded BF-PP composites containing 40 wt% BF and using 2 wt% of MAPP compatibilizer (i.e., $8.49 \pm 0.36 \text{ kJ/m}^2$).

3.5.1 | Effect of infill density

The effect of infill density on Young's modulus in the 35BF65PP and 45BF55PP 3D printed composites is presented in Figure 11. It is seen that, for the 45BF55PP formulation, the increase of infill density improves the

Mr. Spencer H. Lowder and Mr. Rajan Adhikari for their assistance in conducting tensile tests and to the Franceschi Microscopy Center, WSU.

mechanical properties. However, no visible effect is identified in the 35BF65PP composite, due probably to the slight change in the weight of the composite because of the small size of the tensile specimens. The use of high infill densities, with improved Young's modulus, could be of interest for some applications where the increased weight of the 3D printed part is not a limitation. This work shows the promising prospect of integrating basalt fiber as a filler to manufacture BF-PP composites, highlighting their ease of production through 3D printing processes.

4 | CONCLUSION

Basalt fiber was used as a filler in BF-PP composites and as a potential alternative to carbon fiber and glass fiber for manufacturing PP-based composites via 3D printing. In this work, formulations containing up to 45 wt% BF were successfully 3D printed. The rheological behavior of all formulations suggests approximately similar printability. The BF-PP composites showed better dimensional stability than neat PP since the composites, in all cases, retained their shapes and size during and after the 3D printing process. BF also enhanced the mechanical properties of the composites. Only with higher proportions of BF (over 35%), Young's modulus of 3D printed composites increased by up to three times compared to that of neat PP specimens, whereas the strength increased only by about 25%. Such an increase can result mainly from an adequate distribution and alignment of BF in the composite and, marginally, from the interaction of silanesized BF with the PP matrix; however, a more effective sizing of BF is needed to improve the interaction between PP and BF. The reinforcing role of BF in PP-based composites is verified since PP is known for its poor mechanical properties. Izod impact resistance of the composites containing 45 wt% BF retained no less than 70% the impact resistance of 3D-printed neat PP. The mechanical properties of the composites vary depending on the percentage of BF utilized, enabling the production of BF-PP composites to be tuned to meet the specific requirements of the final application. Therefore, BF-PP composites show potential for applications where neat PP use is limited due to poor mechanical properties and difficulty in controlling dimensional stability (warping) during 3D printing processes.

ACKNOWLEDGMENTS

This research was partially funded by the National Science Foundation (grant number 1738669). We acknowledge Sudaglass Fiber Technologies and RheTech for providing basalt fiber and polypropylene, respectively. Thanks to

DATA AVAILABILITY STATEMENT

The data that support the findings of this study are available from the corresponding author upon reasonable request.

ORCID

Vikram Yadama https://orcid.org/0000-0002-2741-9149

REFERENCES

- 1. Chen Y, Awasthi AK, Wei F, Tan Q, Li J. Single-use plastics: production, usage, disposal, and adverse impacts. *Sci Total Environ*. 2021;752:141772. doi:10.1016/j.scitotenv.2020.141772
- Carneiro OS, Silva AF, Gomes R. Fused deposition modeling with polypropylene. *Mater des.* 2015;83:768-776. doi:10.1016/j. matdes.2015.06.053
- Chirayil CJ, Joy J, Maria HJ, Krupa I, Thomas S. Polyolefins in Automotive Industry. 2016:265–283. doi:10.1007/978-3-319-25982-6_11
- Al-Ali AlMa'adeed M, Krupa I. Introduction. 2016:1–11. doi:10. 1007/978-3-319-25982-6_1
- Stoof D, Pickering K. Sustainable composite fused deposition modelling filament using recycled pre-consumer polypropylene. Compos B Eng. 2018;135:110-118. doi:10.1016/j.compositesb.2017. 10.005
- Kwon DJ, Kim NSR, Jang YJ, et al. Investigation of impact resistance performance of carbon fiber reinforced polypropylene composites with different lamination to applicate fender parts. Compos B Eng. 2021;215:108767. doi:10.1016/j. compositesb.2021.108767
- Pickering KL, Beckermann GW, Alam SN, Foreman NJ. Optimising industrial hemp fibre for composites. *Compos Part A Appl Sci Manuf.* 2007;38(2):461-468. doi:10.1016/j.compositesa. 2006.02.020
- Nourbakhsh A, Ashori A. Wood plastic composites from agrowaste materials: analysis of mechanical properties. *Bioresour Technol*. 2010;101(7):2525-2528. doi:10.1016/j.biortech.2009.11.040
- Yang HS, Gardner DJ, Nader JW. Characteristic impact resistance model analysis of cellulose nanofibril-filled polypropylene composites. *Compos Part A Appl Sci Manuf.* 2011;42(12): 2028-2035. doi:10.1016/j.compositesa.2011.09.009
- Koronis G, Silva A, Fontul M. Green composites: A review of adequate materials for automotive applications. *Compos B Eng.* 2013;44(1):120-127. doi:10.1016/j.compositesb.2012.07.004
- 11. Jarukumjorn K, Suppakarn N. Effect of glass fiber hybridization on properties of sisal fiber–polypropylene composites. *Compos B Eng.* 2009;40(7):623-627. doi:10.1016/j.compositesb. 2009.04.007
- 12. Guo G, Chen JC, Gong G. Injection molding of polypropylene hybrid composites reinforced with carbon fiber and wood fiber. *Polym Compos.* 2018;39(9):3329-3335. doi:10.1002/pc.24350
- 13. Purohit A, Satapathy A. Development and performance analysis of wear resistant polypropylene composites filled with micro sized Linz–Donawitz sludge particulates. *Polymers and Polymer Composites*. 2021;29(9_suppl):S1235-S1247. doi:10. 1177/09673911211051569

- 14. Purohit A, Gupta G, Pradhan P, Agrawal A. Development and erosion wear analysis of polypropylene/Linz-Donawitz sludge composites. *Polym Compos*. 2023;44(10):6556-6565. doi:10. 1002/pc.27579
- Ratanawilai T, Taneerat K. Alternative polymeric matrices for wood-plastic composites: effects on mechanical properties and resistance to natural weathering. *Construct Build Mater.* 2018; 172:349-357. doi:10.1016/j.conbuildmat.2018.03.266
- Ngo TD, Kashani A, Imbalzano G, Nguyen KTQ, Hui D. Additive manufacturing (3D printing): A review of materials, methods, applications and challenges. *Compos B Eng.* 2018;143: 172-196. doi:10.1016/j.compositesb.2018.02.012
- Caminero MA, Chacón JM, García-Moreno I, Rodríguez GP. Impact damage resistance of 3D printed continuous fibre reinforced thermoplastic composites using fused deposition modelling. *Compos B Eng.* 2018;148:93-103. doi:10.1016/j.compositesb. 2018.04.054
- Ivey M, Melenka GW, JasonP C, Ayranci C. Characterizing shortfiber-reinforced composites produced using additive manufacturing. Advanced Manufacturing: Polymer & Composites Science. 2017;3(3):81-91. doi:10.1080/20550340.2017.1341125
- Sang L, Han S, Li Z, Yang X, Hou W. Development of short basalt fiber reinforced polylactide composites and their feasible evaluation for 3D printing applications. *Compos B Eng.* 2019; 164:629-639. doi:10.1016/j.compositesb.2019.01.085
- Chang YC, Chen Y, Ning J, et al. No such thing as trash: A 3D-printable polymer composite composed of oil-extracted spent coffee grounds and Polylactic acid with enhanced impact toughness. ACS Sustain Chem Eng. 2019;7(18):15304-15310. doi:10.1021/acssuschemeng.9b02527
- 21. Sanei SHR, Popescu D. 3D-printed carbon fiber reinforced polymer composites: A systematic review. *Journal of Composites Science*. 2020;4(3):98. doi:10.3390/jcs4030098
- Tekinalp HL, Kunc V, Velez-Garcia GM, et al. Highly oriented carbon fiber–polymer composites via additive manufacturing. *Compos Sci Technol*. 2014;105:144-150. doi:10.1016/j. compscitech.2014.10.009
- 23. Ning F, Cong W, Qiu J, Wei J, Wang S. Additive manufacturing of carbon fiber reinforced thermoplastic composites using fused deposition modeling. *Compos B Eng.* 2015;80:369-378. doi:10. 1016/j.compositesb.2015.06.013
- Young D, Wetmore N, Czabaj M. Interlayer fracture toughness of additively manufactured unreinforced and carbonfiber-reinforced acrylonitrile butadiene styrene. *Addit Manuf*. 2018;22:508-515. doi:10.1016/j.addma.2018.02.023
- Zhang W, Cotton C, Sun J, et al. Interfacial bonding strength of short carbon fiber/acrylonitrile-butadiene-styrene composites fabricated by fused deposition modeling. *Compos B Eng.* 2018; 137:51-59. doi:10.1016/j.compositesb.2017.11.018
- Ferreira RTL, Amatte IC, Dutra TA, Bürger D. Experimental characterization and micrography of 3D printed PLA and PLA reinforced with short carbon fibers. *Compos B Eng.* 2017;124: 88-100. doi:10.1016/j.compositesb.2017.05.013
- Shulga E, Karamov R, Sergeichev IS, et al. Fused filament fabricated polypropylene composite reinforced by aligned glass fibers. *Materials*. 2020;13(16):3442. doi:10.3390/ ma13163442
- 28. Sodeifian G, Ghaseminejad S, Yousefi AA. Preparation of polypropylene/short glass fiber composite as fused deposition

- modeling (FDM) filament. *Results Phys.* 2019;12:205-222. doi: 10.1016/j.rinp.2018.11.065
- Ghabezi P, Flanagan T, Harrison N. Short basalt fibre reinforced recycled polypropylene filaments for 3D printing. *Mater Lett.* 2022;326:132942. doi:10.1016/j.matlet.2022.132942
- Bertolino M, Battegazzore D, Arrigo R, Frache A. Designing 3D printable polypropylene: material and process optimisation through rheology. *Addit Manuf*. 2021;40:101944. doi:10.1016/j. addma.2021.101944
- 31. Spoerk M, Holzer C, Gonzalez-Gutierrez J. Material extrusion-based additive manufacturing of polypropylene: A review on how to improve dimensional inaccuracy and warpage. *J Appl Polym Sci.* 2020;137(12):48545. doi:10.1002/app.48545
- 32. Chatterjee R, Sk M, Chanda J, et al. How open-stage melt crystallization affects tensile and shrinkage properties of 3D printed polypropylene. *Polym Eng Sci.* 2023;63(9):2985-2998. doi:10.1002/pen.26422
- 33. Austermann J, Kuscera R, Wipperfürth J, Hopmann C, Dahlmann R. Influence of material modification and fillers on the dimensional stability and warpage of polypropylene in screw-extrusion-based large area additive manufacturing. *Polym Eng Sci.* 2023;63(5):1598-1612. doi:10.1002/pen.26309
- 34. Rani M, Choudhary P, Krishnan V, Zafar S. A review on recycling and reuse methods for carbon fiber/glass fiber composites waste from wind turbine blades. *Compos B Eng.* 2021;215: 108768. doi:10.1016/j.compositesb.2021.108768
- Dhand V, Mittal G, Rhee KY, Park SJ, Hui D. A short review on basalt fiber reinforced polymer composites. *Compos B Eng.* 2015;73:166-180. doi:10.1016/j.compositesb.2014.12.011
- Bednarowski D, Bazan P, Kuciel S. Enhancing strength and sustainability: evaluating glass and basalt fiber-reinforced biopolyamide as alternatives for petroleum-based polyamide composite. *Polymers (Basel)*. 2023;15(16):3400. doi:10.3390/polym15163400
- 37. Liu H, Yu Y, Liu Y, et al. A review on basalt fiber composites and their applications in clean energy sector and power grids. *Polymers (Basel)*. 2022;14(12):2376. doi:10.3390/polym14122376
- 38. Torres JP, Hoto R, Andrés J, García-Manrique JA. Manufacture of green-composite Sandwich structures with basalt fiber and bioepoxy resin. *Advances in Materials Science and Engineering*. 2013;2013;1-9. doi:10.1155/2013/214506
- Jamshaid H, Mishra R. A green material from rock: basalt fiber – a review. *The Journal of the Textile Institute*. 2016;107(7): 923-937. doi:10.1080/00405000.2015.1071940
- 40. Grau F, Choo H, Hu J, Jung J. Engineering behavior and characteristics of wood ash and sugarcane bagasse ash. *Materials*. 2015;8(10):6962-6977. doi:10.3390/ma8105353
- 41. Coughlin N, Drake B, Fjerstad M, et al. Development and mechanical properties of basalt fiber-reinforced acrylonitrile butadiene styrene for in-space manufacturing applications. *Journal of Composites Science*. 2019;3(3):89. doi:10.3390/jcs3030089
- Deng X, Hoo MS, Cheah YW, Tran LQN. Processing and mechanical properties of basalt fibre-reinforced thermoplastic composites. *Polymers (Basel)*. 2022;14(6):1220. doi:10.3390/ polym14061220
- 43. Saleem A, Medina L, Skrifvars M. Mechanical performance of hybrid bast and basalt fibers reinforced polymer composites. *Journal of Polymer Research*. 2020;27(3):61. doi:10.1007/s10965-020-2028-6

- 44. Dao TT, Ye AX, TaA S, Roye N, Hedman K. Capillary Rheometry: analysis of low-viscosity fluids, and viscous liquids and melts at high shear rates. Am Lab. 2019. https://www. americanlaboratory.com/913-Technical-Articles/557-Capillary-Rheometry-Analysis-of-Low-Viscosity-Fluids-and-Viscous-Liquidsand-Melts-at-High-Shear-Rates/
- 45. Rhodes K, Pelaez-Samaniego MR, Kiziltas A, et al. Mechanical and viscoelastic properties of basalt-hemp hybrid reinforced polypropylene. Journal of Thermoplastic Composite Materials. 2023;37 (1):336-362. doi:10.1177/08927057231177249
- 46. Abdelwahab MA, Rodriguez-Uribe A, Misra MK, Mohanty A. Injection molded novel biocomposites from polypropylene and sustainable biocarbon. Molecules. 2019;24(22):4026. doi:10. 3390/molecules24224026
- 47. Schwab A, Levato R, D'Este M, Piluso S, Eglin D, Malda J. Printability and shape Fidelity of bioinks in 3D bioprinting. Chem Rev. 2020;120(19):11028-11055. doi:10.1021/acs.chemrev.0c00084
- Patti A, Acierno S, Nele L, Graziosi L, Acierno D. Sustainable basalt fibers versus traditional glass fibers: comparative study on thermal properties and flow behavior of polyamide 66-based

- ChemEngineering. 2022;6(6):86. composites. chemengineering6060086
- 49. Yang BX, Shi JH, Pramoda KP, Goh SH. Enhancement of the mechanical properties of polypropylene using polypropylene-grafted multiwalled carbon nanotubes. Compos Sci Technol. 2008;68(12):2490-2497. doi:10.1016/j. compscitech.2008.05.001
- 50. Le Bozec Y, Kaang S, Hine PJ, Ward IM. The thermal-expansion behaviour of hot-compacted polypropylene and polyethylene composites. Compos Sci Technol. 2000;60(3):333-344. doi:10.1016/ S0266-3538(99)00129-3

How to cite this article: Pelaez-Samaniego MR, Rhodes K, Garcia-Perez T, et al. Basalt fiber reinforced polypropylene to manufacture 3D printed composites. Polym Compos. 2024;45(13): 12362-12376. doi:10.1002/pc.28641